Simultaneous assessment of microcalcifications and morphological criteria of vulnerability in carotid artery plaque using hybrid 18F-NaF PET/MRI

Laura Mechtouff, Monica Sigovan, Philippe Douek, Nicolas Costes, Didier Le Bars, Adeline Mansuy, Julie Haesebaert, Alexandre Bani-Sadr, Jérémie Tordo, Patrick Feugier, et al.

Simultaneous assessment of microcalcifications and morphological criteria of vulnerability in carotid artery plaque using hybrid ^{18}F-NaF PET/MRI

Laura Mechtouff,[a,b] Monica Sigovan,[c,d] Philippe Douek,[c,d,e] Nicolas Costes,[f] Didier Le Bars,[f,g] Adeline Mansuy,[h] Julie Haesebaert,[i] Alexandre Bani-Sadr,[j] Jérémie Tordo,[j] Patrick Feugier,[k] Antoine Millon,[k] Stéphane Luong,[e] Salim Si-Mohamed,[e] Diane Collet-Benzaquen,[l] Emmanuelle Canet-Soulas,[b] Thomas Bochaton,[b] Claire Crola Da Silva,[b] Alexandre Paccalet,[b] David Magne,[m] Yves Berthezene,[c,n] and Norbert Nighoghossian[a,b]

[a] Stroke Department, Pierre Wertheimer Hospital, Hospices Civils de Lyon, Bron, France
[b] INSERM U1060, CarMeN Laboratory, University Lyon 1, Lyon, France
[c] CNRS, UMR 5220, CREATIS, University of Lyon, Lyon, France
[d] INSA-Lyon UCBL, Inserm U1206, UJM-Saint Etienne, Lyon, France
[e] Department of Radiology, Louis Pradel University Hospital, Bron, France
[f] CERMEP - Imagerie du vivant, Lyon, France
[g] ICBMS, University C. Bernard Lyon 1 & Hospices Civils de Lyon, Lyon, France
[h] Cellule Recherche Imagerie, Louis Pradel University Hospital, Bron, France
[i] Clinical Research and Epidemiology Unit, Public Health Department Hospices Civils de Lyon & Université de Lyon, Université Claude Bernard Lyon 1, Université Saint-Étienne, HESPER EA 7425, F-69008 Lyon, Saint-Etienne, France
[j] Department of Nuclear Medicine, Lyon Sud Hospital, Hospices Civils de Lyon, Lyon, France
[k] Vascular Surgery Department, Edouard Herriot University Hospital & Claude Bernard Lyon 1 University, Lyon, France
[l] Laboratoire d'Anatomie et de Cytologie pathologiques Technipath, Limonest, France
[m] ICBMS, CNRS, UMR 5246, University Lyon 1, Lyon, France
[n] Neuroradiology Department, Pierre Wertheimer Hospital, Bron, France

Received Apr 13, 2020; accepted Aug 28, 2020
doi:10.1007/s12350-020-02400-0

Background. **Previous studies have suggested the role of microcalcifications in plaque vulnerability. This exploratory study sought to assess the potential of hybrid positron-emission tomography (PET)/magnetic resonance imaging (MRI) using ^{18}F-sodium fluoride (^{18}F-NaF) to check simultaneously ^{18}F-NaF uptake, a marker of microcalcifications, and morphological criteria of vulnerability.**

Methods and results. **We included 12 patients with either recently symptomatic or asymptomatic carotid stenosis. All patients underwent ^{18}F-NaF PET/MRI. ^{18}F-NaF target-to-**

Electronic supplementary material The online version of this article (https://doi.org/10.1007/s12350-020-02400-0) contains supplementary material, which is available to authorized users.

The authors of this article have provided a PowerPointfile, available for download at SpringerLink, which summarises thecontents of the paper and is free for re-use at meetings andpresentations. Search for the article DOI on SpringerLink.com.

Theauthors have also provided an audio summary of the article, which isavailable to download as ESM, or to listen to via the JNC/ASNCPodcast.

Reprint requests: Laura Mechtouff, Stroke Department, Pierre Wertheimer Hospital, Hospices Civils de Lyon, 59 Boulevard Pinel, 69677 Bron, France; *laura.mechtouff@chu-lyon.fr*

1071-3581/$34.00

Published online: 03 November 2020

background ratio (TBR) was measured in culprit and nonculprit (including contralateral plaques of symptomatic patients) plaques as well as in other arterial walls. Morphological criteria of vulnerability were assessed on MRI. Mineral metabolism markers were also collected. ^{18}F-NaF uptake was higher in culprit compared to nonculprit plaques (median TBR 2.6 [2.2-2.8] vs 1.7 [1.3-2.2]; P = 0.03) but was not associated with morphological criteria of vulnerability on MRI. We found a positive correlation between ^{18}F-NaF uptake and calcium plaque volume and ratio but not with circulating tissue-nonspecific alkaline phosphatase (TNAP) activity and inorganic pyrophosphate (PPi) levels. ^{18}F-NaF uptake in the other arterial walls did not differ between symptomatic and asymptomatic patients.

Conclusions. **^{18}F-NaF PET/MRI may be a promising tool for providing additional insights into the plaque vulnerability. (J Nucl Cardiol 2020)**

Key Words: Carotid stenosis • Positron-Emission Tomography-Computed Tomography • Hybrid MR/PET • Sodium Fluoride • Stroke

Abbreviations

^{18}F-NaF	^{18}F-sodium fluoride
AP	Alkaline phosphatase
BMI	Body mass index
BW	Bandwidth
CE-MRA	Contrast-enhanced
CRP	C-reactive protein
CT	Computed tomography
DUS	Doppler ultrasound
FC	Fibrous cap
FLASH	Fast-low angle shot
FOV	Field of view
IPH	Intraplaque hemorrhage
IQR	Interquartile range
LDL	Low-density lipoprotein
LRNC	Lipid-rich necrotic core
MR	Angiography
MRI	Magnetic resonance imaging
NA	Number of averages
NASCET	North American Symptomatic Carotid Endarterectomy Trial
NIHSS	National institutes of health stroke scale
PET	Positron-emission tomography
PPi	Inorganic pyrophosphate
ROI	Region of interest
SD	Standard Deviation
SPAIR	Spectral attenuated inversion recovery
SUVmax	Maximum standard uptake value
TE	Echo time
TBR	Target-to-background ratio
TIA	Transient ischemic attack
TNAP	Tissue-nonspecific alkaline phosphatase
TOF	Time-of-flight angiography
TR	Repetition time
VSMC	Vascular smooth muscle cell

INTRODUCTION

Atherosclerotic stenosis of the extracranial carotid artery accounts for 15 to 20% of ischemic strokes.[1] Beyond the degree of stenosis, plaque vulnerability and subsequent thromboembolic events are related to a combination of factors that include a large lipid-rich necrotic core (LRNC), a thinning/ruptured fibrous cap (FC), an intraplaque hemorrhage (IPH), and inflammatory processes.[2,3] Identifying high-risk plaques is therefore critical for improving both risk prediction and prevention of ischemic stroke.

The formation and progression of atherosclerotic plaques are a dynamic process that includes macrophage-driven inflammation and calcifications, two related but distinct processes. Until now, in vivo exploration of plaque inflammatory processes has been mostly explored by the use of ^{18}F-fluorodesoxyglucose (^{18}F-FDG), a known marker of vascular macrophage burden.[4–9] ^{18}F-sodium fluoride (^{18}F-NaF) positron-emission tomography (PET) has recently been proposed as a technique to detect microcalcifications, a key component of the inflammatory process within plaques.[10] The use of this latter radiotracer adds additional information as evidenced by the fact that arterial ^{18}F-FDG retention is not correlated with arterial ^{18}F-NaF uptake.[11–13] Studies on coronary arteries have shown that ^{18}F-NaF uptake was higher in culprit lesions of acute myocardial infarction than in nonculprit lesions.[14,15] Other studies found that ^{18}F-NaF uptake localized high-risk plaques in asymptomatic patients using optical coherence tomography, intravascular ultrasound, and coronary computed tomography angiography.[16,17] In carotid arteries, results of preliminary studies using ^{18}F-NaF-PET/computed tomography (CT) have suggested an association between ^{18}F-NaF uptake and the symptomatic nature of carotid plaques.[11,14,15,18–21]

Among the noninvasive imaging techniques available today, carotid plaque MRI is able to detect

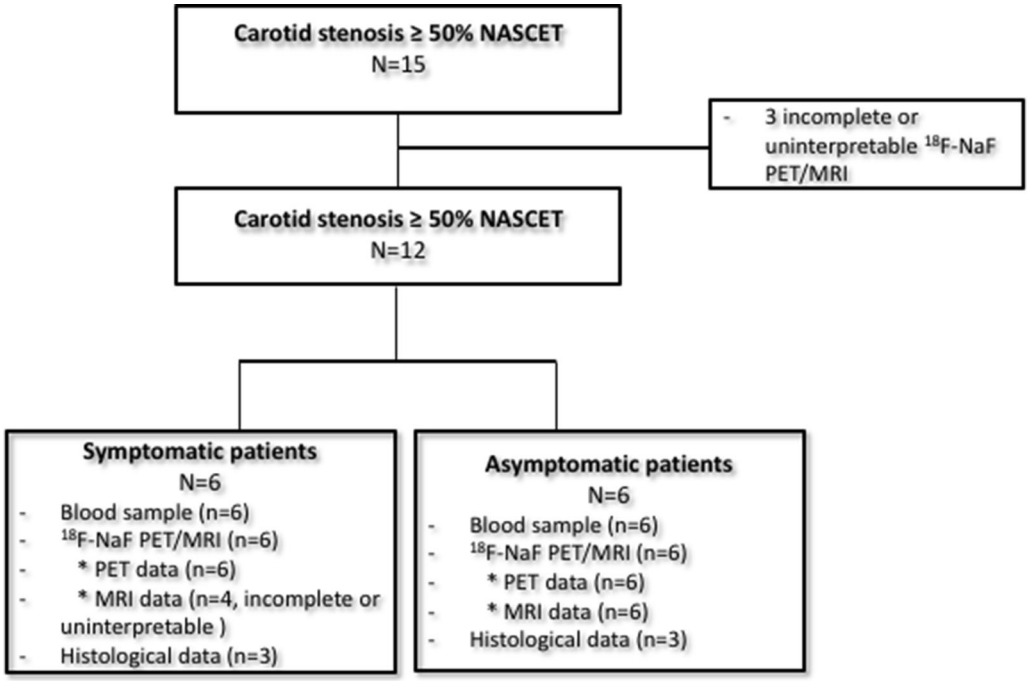

Figure 1. Study flow diagram (NASCET: North American Symptomatic Carotid Endarterectomy Trial, ^{18}F-NaF PET/MRI PET: ^{18}F-sodium fluoride positron-emission tomography/magnetic resonance).

morphological changes underlying plaque vulnerability with moderate-to-good sensitivity and specificity compared to histological findings.[22,23] Thus, hybrid ^{18}F-NaF PET/MRI is able to simultaneously assess ^{18}F-NaF uptake, a marker of microcalcifications, and morphological criteria of vulnerability and may therefore provide additional insights into plaque vulnerability.

Experimental studies have demonstrated that tissue-nonspecific alkaline phosphatase (TNAP) is a key determinant of tissue calcification.[24] In hydrolyzing inorganic pyrophosphate (PPi), one of the main inhibitors of calcification, it contributes to the formation of hydroxyapatite crystals. Higher levels of serum alkaline phosphatase (AP) are associated with the increased risk of all-cause and cardiovascular mortality among survivors of myocardial infarction or stroke and in a general population sample.[25,26]

The aim of this study was to investigate if ^{18}F-NaF uptake—assessed using hybrid ^{18}F-NaF PET/MRI—differed between culprit and nonculprit carotid plaques. Secondary aim ignored the symptomatic nature of the plaque and compared TBR and morphological criteria of vulnerability on MRI or mineral metabolism markers (TNAP and PPi). We also compared ^{18}F-NaF uptake in other arterial walls in symptomatic and asymptomatic patients.

MATERIALS AND METHODS

Study Population

Patients were prospectively recruited between January 2016 and December 2017 from the stroke department and the department of vascular surgery in Lyon, France. Patients with carotid stenosis ($\geq$ 50% according to the North American Symptomatic Carotid Endarterectomy Trial (NASCET) criteria) were included and classified as symptomatic (transient ischemic attack (TIA) or minor stroke $\leq$ 15 days) or asymptomatic.[27] Culprit plaques were plaques recently responsible for ipsilateral transient ischemic attack or minor stroke $\leq$ 15 days. Nonculprit plaques were contralateral plaques of symptomatic patients and plaques of asymptomatic patients. Indication for carotid endarterectomy was decided by a surgeon expert panel according to current guidelines.[28] Exclusion criteria were ongoing pregnancy, severe renal failure (estimated glomerular filtration rate by the Cockroft-Gault formula $<$ 50 ml/min), metallic implants, and severe claustrophobia.

Clinical history, common risk factors, Doppler ultrasound (US), CT angiography data including calcium volume and ratio into the plaque, and routine biological markers drawn the same day including calcemia, phosphoremia, and C-reactive protein (CRP)

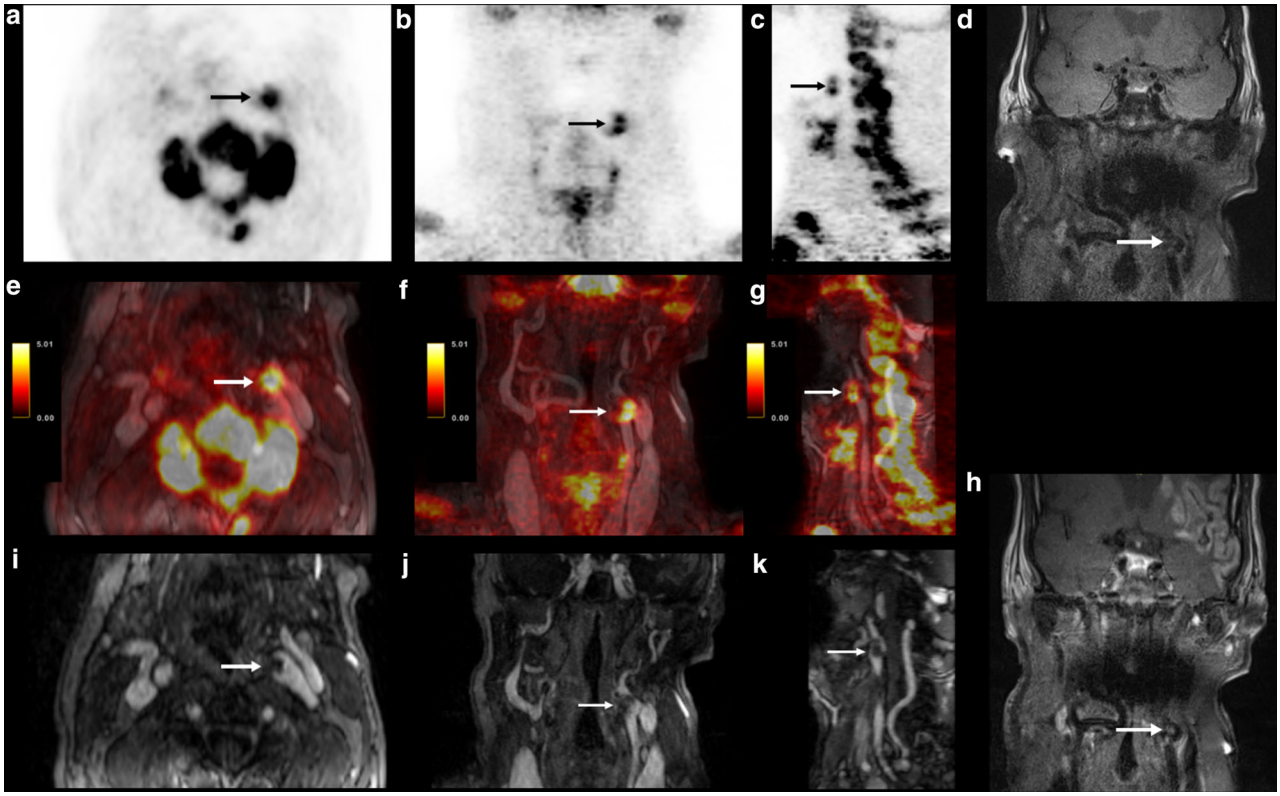

Figure 2. ^{18}F-sodium fluoride positron-emission tomography/magnetic resonance (^{18}F-NaF PET/MRI) PET/MRI from a 59-year-old patient (No. 11) who experienced right hemiparesis and aphasia related to left middle cerebral artery territory infarct. Axial, coronal, and sagittal views of PET (**A**–**C**) showing ^{18}F-NaF uptake into the left carotid plaque (black arrow). Axial, coronal, and sagittal views of merged PET/MRI (**E**–**G**) images showing ^{18}F-NaF uptake overlayed on the T1-w images (black arrow); Axial, coronal, and sagittal views of contrast-enhanced angiography (**I**–**K**) showing an eccentric plaque of the left carotid artery causing a luminal stenosis; Coronal T1-weighted MR images pre- and post-gadolinium showing a macrocalcification and a focal enhancement of the plaque (**D**, **H**).

were collected. When carotid endarterectomy was indicated, histological analyses of the plaques were performed.

The study protocol was registered at the ClinicalTrials.gov online database (NCT02726984), with the approval of the local research ethics committee in accordance with the declaration of Helsinki. All patients provided written informed consent before enrollment.

^{18}F-NaF PET–MRI

PET/MRI Protocol All patients underwent PET/MRI. The 15 min PET acquisition was centered on the carotid arteries and was performed 60 min after injection of 3 MBq/kg of ^{18}F-NaF.

The 3T MR multi-contrast protocol consisted of a 3D time-of-flight angiography (TOF), a 3D T1-weighted variable flip angle turbo spin echo (SPACE) sequence, and a 3D contrast-enhanced angiography (CE-MRA) performed during the first passage of 30 cm^3 of a Gadolinium-based contrast agent (DOTAREM©, Guerbet, France), administered at 2 cm^3/s, followed by a 10 cm^3 saline flush.

The following TOF sequence was performed: repetition time/echo time (TR/TE) 21.0/3.60 ms, flip angle 25°, field of view (FOV) 200 × 150 × 30 mm, slice thickness 0.7 mm, in-plane resolution 0.7 × 0.6 mm, number of averages (NA) 1, acquisition bandwidth (BW) 252 Hz/pixel, parallel imaging (GRAPPA) acceleration factor in the phase-encoding direction: 2, and scan time: approximately 3 min.

The 3D SPACE sequence was performed in the coronal orientation using a spectral attenuated inversion recovery (SPAIR) fat suppression pulse with the following parameters: TR/TE 800/22 ms, voxel 0.7 mm

Table 1. Patient baseline characteristics

	Symptomatic patients (n = 6)	Asymptomatic patients (n = 6)	P value
Age, y	72 [59-78]	72 [63-75]	0.94
Male	5 (83.3)	4 (66.7)	1.00
Qualifying event			
TIA	2 (33.3)	-	-
Ischemic stroke	4 (66.7)	-	-
Baseline NIHSS	2 [0-4]	-	-
Hypertension	5 (83.3)	3 (50)	0.55
Diabetes	1 (16.7)	1 (16.7)	0.77
Hyperlipidemia	4 (66.7)	2 (33.3)	0.57
Current smoking	1 (16.7)	1 (16.7)	1.00
BMI, kg/m^2	28.2 [25.0-29.4]	25.1 [23.0-26.9]	0.11
Coronary artery disease	1.0 (0.7)	2 (33.3)	1.00
Atrial fibrillation	2 (33.3)	0	0.45
LDL-cholesterol, g/L	1.2 [0.8-1.2]	1.3 [0.4-1.5]	0.87
CRP, mg/L	3.8 [1.2-15.0]	1.7 [0.8-3.1]	0.17
Calcemia, mmol/L	2.3 [2.1-2.3]	2.4 [2.3-2.4]	0.03
Phosphoremia, mmol/L	1.1 [0.9-1.1]	1 [1.0-1.1]	0.75
TNAP activity, nmol/min/mg	0.08 [0.06-0.15]	0.08 [0.07-0.12]	0.75
PPI, μM	9.1 [6.8-12.2]	10.6 [7.2-14.7]	0.42

TIA transient ischemic attack; *NIHSS* National Institutes of Health Stroke Scale; *BMI* body mass index; *LDL* low-density lipoprotein; *CRP* C-reactive protein; *TNAP* tissue-nonspecific alkaline phosphatase; *PPi* inorganic pyrophosphate
Variables are displayed as absolute number (percentage of column total), mean ± SD, or median (25th–75th percentiles) as appropriate

isotropic, turbo factor 55, TSE echo spacing/shot duration 4.32/238 ms, BW 630 Hz/pixel, NA 1.4, GRAPPA acceleration factor in the phase-encoding direction: 2, and scan time of 6.16 min.

CE-MRA coronal images were acquired in the coronal orientation using a 3D T1-weighted fast low-angle shot (FLASH) sequence with the following parameters: TR/TE 3.13/1.16 ms, Field of view (FOV) 480 × 427 mm, fractional anisotropy (FA) 25°, 88 slices of 1 mm, in-plane resolution: 1.1 × 0.9 mm, GRAPPA acceleration factor in the phase-encoding direction: 2, BW 650 Hz/pixel, 3D- centric reordering with time to center of k-space: 1 s, NA 1, and scan time of 31 s. The 3D T1-weighted SPACE acquisition was repeated after contrast injection to evaluate contrast uptake in the plaque.

Image Analysis MRI was assessed for morphological criteria of vulnerability, only for plaque with stenosis ≥ 50%. The maximum standard uptake value (SUVmax) (the decay-corrected tissue concentration of the tracer divided by the injected dose per body weight) was measured using 3 regions of interest (ROI) centered on the area of highest uptake in the plaque identified on coregistered PET/MRI fusion images. If there was no plaque, on the contralateral carotid, the ^{18}F-NaF uptake in the proximal 1 cm of internal carotid artery, just distal to the bifurcation was quantified. ^{18}F-NaF uptake was also quantified in other artery walls as aortic arch, ostium of brachiocephalic trunk, left subclavian artery, and left common carotid artery using MRI data. Blood-pool SUV was estimated as the mean of five ROIs in the mid lumen of the superior vena cava. The target-to-background ratio (TBR) was calculated by dividing SUVmax by the blood-pool SUV. Two experienced raters reviewed PET/MRI and estimated the ^{18}F-NaF TBR blinded to clinical data (J. T. and A. B-S.).

Blood Sampling Protocol

A peripheral blood sample was collected from each patient the same day as the ^{18}F-NaF PET/MRI. Sera were prepared and stored at − 80°C within a 3-h delay at the NeuroBioTec biobank (CRB-HCL: BB-0033-00046, France). All samples were thawed only once for

Table 2. Plaque imaging and histological characteristics in culprit and nonculprit plaques

	Culprit plaques (n = 6)	Non culprit plaques (n = 18)	P value
CT angiography			
Calcium volume, mm3	462 [88-843]	105 [0-474]	0.19
Calcium volume, %	35.6 [5.3-78.9]	21.9 [0-59]	0.51
MRI			
Intraplaque hemorrhage	2 (50)	2 (11.1)	0.14
Lipid-rich necrotic core	2 (50)	3 (16.7)	0.21
Thinning and/or ruptured fibrous cap	1 (25)	5 (27.8)	1.00
^{18}F-NaF uptake			
SUV max, g/mL	4.2 [1.8-5.9]	2.3 [1.8-3.1]	0.18
TBR	2.6 [2.2-2.8]	1.7 [1.3-2.2]	0.03
Histological exam			
Intraplaque hemorrhage	3 (100)	2 (66.7)	1.00
Lipid-rich necrotic core	3 (100)	3 (100)	-
Thinning and/or ruptured fibrous cap	3 (100)	3 (100)	-
Microcalcifications	3 (100)	3 (100)	-
Inflammatory cells	2 (66.7)	3 (100)	1.00
Neoangiogenesis	1 (33.3)	3 (100)	0.4

^{18}F-NaF ^{18}F-sodium fluoride; *SUV* standard uptake value; *TBR* target-to-background ratio
Variables are displayed as absolute number (percentage of column total), mean ± SD, or median (25th–75th percentiles) as appropriate

study measurements. Serum samples were diluted at 1/25. TNAP activity (nmol/min/mg) was quantified by the absorbance of para-nitrophenol generated by TNAP hydrolysis of para-nitrophenylphosphate. PP_i levels (μM) were determined by luminescence using the PP_i light inorganic pyrophosphate assay kit from Lonza. Sensitivity was 0.02 μM.

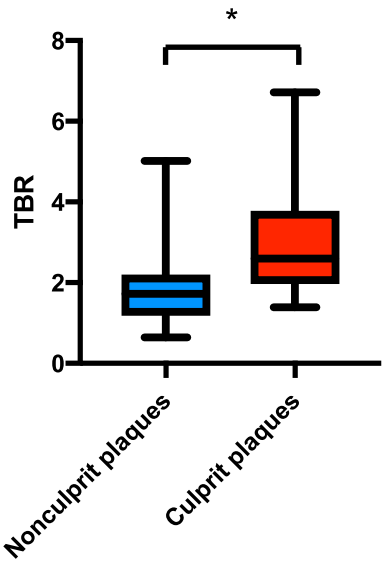

Figure 3. ^{18}F-sodium fluoride (^{18}F-NaF) uptake in culprit (N = 6) vs nonculprit (N = 18) plaques. Box and Whisker Plot.

Histological Analyses

Vessels were fixed in buffered formalin and embedded in paraffin after decalcification. Transverse sections of 3 μm were cut using a rotary microtome (Leica Microsystems GmbH, Wetzlar, Germany) and stained with hematoxylin, phloxine, and saffron in order to analyze the following elements: lipid core, plaque hemorrhage, cap fibroatheroma (thin or thick), microcalcifications, inflammation, thrombi, and neoangiogenesis.

Statistical Analysis

This study was designed as a pilot transversal investigation. The primary analysis was the comparison of ^{18}F-NaF TBR in carotid culprit plaques and nonculprit plaques. Secondary analysis ignored the symptomatic nature of the plaque and compared ^{18}F-NaF TBR and morphological criteria of vulnerability on MRI as well as mineral metabolism markers. We also compared ^{18}F-NaF TBR in the other artery walls in symptomatic and asymptomatic patients. Categorical

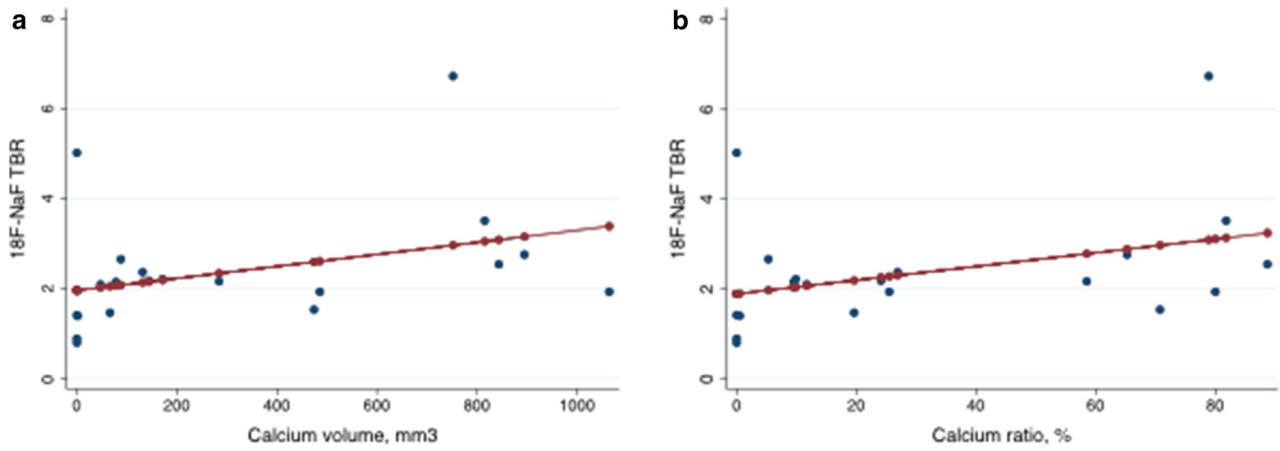

Figure 4. ^{18}F-sodium fluoride uptake with respect to calcium volume (**A**) and calcium ratio (**B**) (^{18}NaF, ^{18}sodium fluoride; TBR, target-to-background ratio). Scatter Plot.

Table 3. ^{18}F-sodium fluoride (^{18}F-NaF) uptake in other arterial walls in symptomatic and asymptomatic patients

	Symptomatic patients (n = 6)	Asymptomatic patients (n = 6)	P value
Aorta	1.0 [0.5-1.4]	1.0 [0.7-1.2]	0.81
Brachiocephalic trunk	1.4 [1.1-1.8]	1.3 [1.1-1.4]	0.52
Left subclavian artery	1.2 [1.2-1.5]	1.2 [1.0-1.3]	0.75
Left common carotid artery	1.1 [0.7-1.2]	1.0 [0.7-1.2]	0.75

Variables are displayed as median (25th–75th percentiles) Target-to-background ratio

variables are presented as numbers and relative frequencies (percentages), and continuous variables as medians with interquartile ranges (IQR). Normality of distributions was assessed graphically and with the Shapiro–Wilk test. All probability values were 2 sided, and values of $P < 0.05$ were considered statistically significant. Fisher's test was used to analyze categorical variables and the Mann–Whitney U test for continuous variables. Correlation was undertaken with Spearman's ρ. Inter-observer reproducibility of ^{18}F-NaF uptake measurements was determined using intraclass correlation coefficient. All analyses were performed using Stata/IC (ACADEMIC/L, SCIC, L1Wi0H,E).

RESULTS

Baseline Characteristics of Patients and Plaques

Fifteen patients were included between 15/01/2016 and 11/12/2017. Three patients were excluded because of incomplete or uninterpretable PET/MRI (Figure 1). Two others had PET imaging but incomplete or uninterpretable MRI. The final sample included 6 symptomatic and 6 asymptomatic patients. Their mean age was 68 years (± 10), and seventy-five percent of the patients were men. Among the six symptomatic patients, 4 had minor ischemic stroke and 2 had TIA. The main characteristics of the symptomatic and asymptomatic patients and the main characteristics of culprit and nonculprit plaques are presented in Tables 1 and 2 and Online Resource 1. Calcemia was slightly higher in asymptomatic patients compared to symptomatic patients (median calcemia 2.4 mmol/L [2.3-2.4] vs 2.3 mmol/L [2.1-2.3]; P = 0.03). Six patients, 3 symptomatic and 3 asymptomatic, underwent carotid endarterectomy through the eversion procedure. All retrieved plaques contained microcalcifications and their histological results are detailed in Table 2.

^{18}F-NaF UPTAKE IN CULPRIT AND NONCULPRIT PLAQUES

The mean delay between symptoms and PET–MRI was 9.2 days (± 6.2). ^{18}F-NaF uptake was higher in culprit plaques compared to nonculprit plaques (median TBR 2.6 [2.2-2.8] vs 1.7 [1.3-2.2]; $P = 0.03$) (Figs. 2, 3 and Table 2). Intraclass correlation coefficient was 0.98.

^{18}F-NaF UPTAKE COMPARED WITH MORPHOLOGICAL CRITERIA OF PLAQUE VULNERABILITY ON MRI AND MINERAL METABOLISM MARKERS

^{18}F-NaF uptake was not associated with morphological criteria of plaque vulnerability on MRI (TBR 1.80 [1.42-2.18] in plaques with IPH vs 1.93 [1.32-2.37] in plaques without IPH; $P = 1.00$; TBR 1.46 [1.45-2.14] in plaques with LRNC vs 1.93 [1.32-2.37] in plaques without LRNC; $P = 0.78$; TBR 1.45 [1.39-1.53] in plaques with thinning and/or ruptured FC vs 2.12 [1.37-2.45] in plaques without thinning and/or ruptured FC; $P = 0.18$). ^{18}NaF uptake was correlated with calcium plaque volume ($\rho = 0.82$; $P < 0.01$) and ratio ($\rho = 0.66$; $P = 0.04$) but was not correlated with circulating TNAP activity or PPi levels (Figure 4).

^{18}F-NaF UPTAKE IN OTHER ARTERY WALLS IN SYMPTOMATIC AND ASYMPTOMATIC PATIENTS

There was no increase of ^{18}F-NaF uptake in the other arterial walls in symptomatic patients compared to asymptomatic patients (Table 3).

BRAIN ^{18}F-NaF UPTAKE

In the 4 patients with stroke, intense ^{18}F-NaF uptake was observed (median TBR = 6.2 [3.8-12.2] vs median TBR = 0.2 [0.1-0.2] for contralateral not infarcted brain; $P = 0.02$).

DISCUSSION

This pilot study was designed to evaluate for the first time the added value of ^{18}F-NaF PET/MRI in the carotid plaques assessment, in checking simultaneously ^{18}F-NaF uptake, a marker of microcalcifications, and morphological criteria of vulnerability on MRI. ^{18}F-NaF uptake was higher in culprit plaques compared to nonculprit plaques in a decoupled way from morphological MRI criteria of vulnerability.

Our results confirm previous results from PET/CT studies in showing a higher ^{18}F-NaF uptake in culprit plaques compared to nonculprit plaques.[11,19] Recent studies also suggested an association between ^{18}F-NaF uptake in carotid plaque and the severity of white matter lesions on brain MRI.[29,30] In contrast, other studies reported different results likely linked to delayed acquisition (180 min after ^{18}F-NaF injection) or delay between symptoms and imaging longer than one month.[18,20,21]

It is increasingly recognized that the type and location, rather than the extent, of calcifications are important in determining atherosclerotic plaque stability. Microcalcification represents the early stages of intimal calcium formation and greatly amplifies mechanical stresses on the surface of the fibrous plaque that may directly contribute to its rupture.[31,32] Simultaneous carotid plaque MRI acquisition appears to be an effective method for assessing their particular impact on plaque vulnerability. In our study, ^{18}F-NaF uptake was decoupled from morphological MRI criteria of vulnerability. That could be linked to the fact that microcalcifications occurred earlier in human plaque development.[2,33] Conversely studies performed with PET/CT for carotid and coronary arteries showed that ^{18}F-NaF uptake was higher in ruptured and high-risk atherosclerotic plaques.[11,16,17] This discrepancy could be explained by the use of different methodological options to define vulnerable plaque.

Histological studies documented that ^{18}F-NaF can detect vascular microcalcification activity and binds only at the surface of large macrocalcifications while CT is able to detect advanced macrocalcification deposits with a diameter of approximately 200-500 μm.[10,11,21] As other authors, we found that ^{18}F-NaF uptake was associated with CT calcium volume and ratio.[10,11,34] By contrast, TNAP activity in the serum was not associated with ^{18}F-NaF uptake, suggesting that circulating TNAP was not involved in the deposition of microcalcifications. This conclusion is strengthened by the fact that circulating TNAP activity was not inversely correlated with PPi levels. We hypothesize that TNAP expressed locally in plaque vascular smooth muscle cells rather than circulating TNAP that participates in plaque calcification. Experiments in mice showed that whereas TNAP overexpression in vascular smooth muscle cells (VSMCs) induced lethal vascular calcification, liver-targeted TNAP overexpression that resulted in strong circulating TNAP activity had no effect.[35,36]

PET–MRI has the added benefit of checking simultaneously neck and thorax arteries. As atherosclerosis is considered as a global inflammatory disease and generalized vulnerability may be more important overall than characterizing the individual sites of vulnerability in the individual patient, we assessed whether ^{18}F-NaF uptake in other arteries may reflect global atherosclerotic activity and if this latter was higher in symptomatic

than in asymptomatic patients.[37,38] This preliminary analysis failed to show any difference between symptomatic and asymptomatic patients but may be biased by the absence of coronary artery tree assessment.

As a previous study using PET/CT, we observed a ^{18}F-NaF uptake within the cerebral infarction.[11] Mechanisms are not completely understood. A recent study has identified an overlap between the pathophysiology of atherosclerosis and liquefactive necrosis related to ischemia in the brain, a lipid-rich organ.[39] Another hypothesis is the passive transfer across the blood–brain barrier.

We recognize some limitations of our study. First, the small sample size in this exploratory study would have prevented us from drawing any statistically significant conclusions regarding the relationship between ^{18}F-NaF uptake and morphological MRI criteria of vulnerability or circulating TNAP and PPi levels, as well as for histological data. Whether ^{18}F-NaF PET/MRI provide additional insights on plaque vulnerability from morphological MRI criteria needs further explorations. Second, the ^{18}F-NaF signal in the plaque may be contaminated by spillover from the spine. To limit this phenomenon, we performed a reconstruction including a point spread function model in the iterative process, which is known to enhance resolution and reduce spillover effects.[40] Furthermore, the attenuation correction with the MRI images is potentially suboptimal since the spine is not present in the computed attenuation maps.[41]

In our preliminary study using hybrid ^{18}F-NaF PET/MRI, ^{18}F-NaF uptake was higher in culprit compared to nonculprit plaques, in a decoupled way from morphological MRI criteria of vulnerability. Thus, ^{18}F-NaF uptake may provide additional insights into the plaque vulnerability and should be considered as a potential surrogate marker of early atherosclerosis.[2,33] The relevance of a risk score combining stenosis and plaque ^{18}F-NaF uptake in predicting clinical events as proposed with ^{18}F-FDG needs further explorations.[42] This study further outlined the complex relationship between plaque activity and circulating biomarkers, confirming the importance of molecular imaging at the lesion site. It could be a relevant tool if new drugs that target microcalcifications process become available, for example, TNAP inhibitors.[43]

NEW KNOWLEDGE GAINED

In this pilot transversal study conducted in symptomatic and asymptomatic patients with carotid stenosis, ^{18}F-NaF uptake was higher in culprit compared to nonculprit plaques, in a decoupled way from morphological MRI criteria of vulnerability, suggesting that hybrid ^{18}F-NaF PET/MRI approach may be a promising tool for providing additional insights into the atherosclerotic plaque vulnerability.

Acknowledgements

We thank Thomas Troalen, application engineer Siemens Healthcare France, for his assistance in the development of the sequences used in this study, Curium for providing 18F-NaF (CISNAF 100 MBq/mL solution for injection, Cis bio international), Karen Reilly for proofreading the English, Morgane Bouin (Cellule Recherche Imagerie) for data collection and the French National 'invest for the future' programs: LILI – Lyon Integrated Life Imaging: hybrid MR-PET ANR-11-EQPX-0026 and CESAME - Brain and Mental Health ANR-10-IBHU-0003. Human biological samples and associated data were obtained from NeuroBioTec (CRB-HCL, Lyon France, Biobank BB-0033-00046).

Disclosure

The authors declare that they have no conflict of interest.

Funding

CREATIS CNRS Lab grant.

References

1. Petty GW, Brown RD, Whisnant JP, Sicks JD, O'Fallon WM, Wiebers DO. Ischemic stroke subtypes: A population-based study of incidence and risk factors. Stroke. 1999;30:2513–6.
2. Stary HC, Chandler AB, Dinsmore RE, Fuster V, Glagov S, Insull W, et al. A definition of advanced types of atherosclerotic lesions and a histological classification of atherosclerosis: A report from the committee on vascular lesions of the council on arteriosclerosis. Am Heart Assoc. Circ. 1995;92:1355–74.
3. Nighoghossian N, Derex L, Douek P. The vulnerable carotid artery plaque: Current imaging methods and new perspectives. Stroke. 2005;36:2764–72.
4. Rudd JHF, Warburton EA, Fryer TD, Jones HA, Clark JC, Antoun N, et al. Imaging atherosclerotic plaque inflammation with [18 F]-fluorodeoxyglucose positron emission tomography. Circulation. 2002;105:2708–11.
5. Davies JR, Rudd JHF, Fryer TD, Graves MJ, Clark JC, Kirkpatrick PJ, et al. Identification of culprit lesions after transient ischemic attack by combined ^{18} F fluorodeoxyglucose positron-emission tomography and high-resolution magnetic resonance imaging. Stroke. 2005;36:2642–7.
6. Tawakol A, Migrino RQ, Bashian GG, Bedri S, Vermylen D, Cury RC, et al. In vivo 18F-fluorodeoxyglucose positron emission tomography imaging provides a noninvasive measure of carotid plaque inflammation in patients. J Am Coll Cardiol. 2006;48:1818–24.
7. Marnane M, Merwick A, Sheehan OC, Hannon N, Foran P, Grant T, et al. Carotid plaque inflammation on 18F-fluorodeoxyglucose positron emission tomography predicts early stroke recurrence. Ann Neurol. 2012;71:709–18.
8. Taqueti VR, Di Carli MF, Jerosch-Herold M, Sukhova GK, Murthy VL, Folco EJ, et al. Increased microvascularization and

vessel permeability associate with active inflammation in human atheromata. Circ Cardiovasc Imaging. 2014;7:920–9.
9. Chowdhury MM, Tarkin JM, Evans NR, Le E, Warburton EA, Hayes PD, et al. 18 F-FDG uptake on PET/CT in symptomatic versus asymptomatic carotid disease: A meta-analysis. Eur J Vasc Endovasc Surg. 2018;56:172–9.
10. Irkle A, Vesey AT, Lewis DY, Skepper JN, Bird JLE, Dweck MR, et al. Identifying active vascular microcalcification by 18F-sodium fluoride positron emission tomography. Nat Commun. 2015;6:7495.
11. Vesey AT, Jenkins WSA, Irkle A, Moss A, Sng G, Forsythe RO, et al. ^{18} F-Fluoride and ^{18} F-fluorodeoxyglucose positron emission tomography after transient ischemic attack or minor ischemic stroke: Case–control study. Circ Cardiovasc Imaging. 2017;10:e004976.
12. Derlin T, Toth Z, Papp L, Wisotzki C, Apostolova I, Habermann CR, et al. Correlation of inflammation assessed by 18F-FDG PET, active mineral deposition assessed by 18F-fluoride PET, and vascular calcification in atherosclerotic plaque: A dual-tracer PET/CT study. J Nucl Med. 2011;52:1020–7.
13. Li X, Heber D, Gonzalez JC, Karanikas G, Mayerhoefer ME, Rasul S, et al. Association between osteogenesis and inflammation during the progression of calcified plaque evaluated by ^{18} F-fluoride and ^{18} F-FDG. J Nucl Med. 2017;58:968–74.
14. Joshi NV, Vesey AT, Williams MC, Shah ASV, Calvert PA, Craighead FHM, et al. 18F-fluoride positron emission tomography for identification of ruptured and high-risk coronary atherosclerotic plaques: A prospective clinical trial. The Lancet. 2014;383:705–13.
15. Adamson PD, Vesey AT, Joshi NV, Newby DE, Dweck MR. Salt in the wound: (18)F-fluoride positron emission tomography for identification of vulnerable coronary plaques. Cardiovasc Diagn Ther. 2015;5:150–5.
16. Lee JM, Bang J-I, Koo B-K, Hwang D, Park J, Zhang J, et al. Clinical relevance of ^{18} F-sodium fluoride positron-emission tomography in noninvasive identification of high-risk plaque in patients with coronary artery disease. Circ Cardiovasc Imaging. 2017;10:e006704.
17. Li L, Li X, Jia Y, Fan J, Wang H, Fan C, et al. Sodium-fluoride PET-CT for the non-invasive evaluation of coronary plaques in symptomatic patients with coronary artery disease: a cross-correlation study with intravascular ultrasound. Eur J Nucl Med Mol Imaging. 2018;45:2181–9.
18. Quirce R, Martínez-Rodríguez I, De Arcocha Torres M, Jiménez-Bonilla JF, Banzo I, Rebollo M, et al. Contribution of 18F-sodium fluoride PET/CT to the study of the carotid atheroma calcification. Rev Esp Med Nucl E Imagen Mol. 2013;32:22–5.
19. Cocker MS, Spence JD, Hammond R, Wells G, deKemp RA, Lum C, et al. [18 F]-NaF PET/CT identifies active calcification in carotid plaque. JACC Cardiovasc Imaging. 2017;10:486–8.
20. Zhang Y, Li H, Jia Y, Yang P, Zhao F, Wang W, et al. Noninvasive assessment of carotid plaques calcification by 18 F-sodium fluoride accumulation: Correlation with pathology. J Stroke Cerebrovasc Dis. 2018;27:1796–801.
21. Hop H, de Boer SA, Reijrink M, Kamphuisen PW, de Borst MH, Pol RA, et al. 18F-sodium fluoride positron emission tomography assessed microcalcifications in culprit and non-culprit human carotid plaques. J Nucl Cardiol. 2019;26:1064–75.
22. den Hartog AG, Bovens SM, Koning W, Hendrikse J, Luijten PR, Moll FL, et al. Current status of clinical magnetic resonance imaging for plaque characterisation in patients with carotid artery stenosis. Eur J Vasc Endovasc Surg. 2013;45:7–21.
23. Saba L, Saam T, Jäger HR, Yuan C, Hatsukami TS, Saloner D, et al. Imaging biomarkers of vulnerable carotid plaques for stroke risk prediction and their potential clinical implications. Lancet Neurol. 2019;18:559–72.
24. Orimo H. The mechanism of mineralization and the role of alkaline phosphatase in health and disease. J Nippon Med Sch Nippon Ika Daigaku Zasshi. 2010;77:4–12.
25. Ryu W-S, Lee S-H, Kim CK, Kim BJ, Yoon B-W. Increased serum alkaline phosphatase as a predictor of long-term mortality after stroke. Neurology. 2010;75:1995–2002.
26. Tonelli M, Curhan G, Pfeffer M, Sacks F, Thadhani R, Melamed ML, et al. Relation between alkaline phosphatase, serum phosphate, and all-cause or cardiovascular mortality. Circulation. 2009;120:1784–92.
27. Barnett HJM. Beneficial effect of carotid endarterectomy in symptomatic patients with high-grade carotid stenosis. N Engl J Med. 1991;325:445–53.
28. Kernan WN, Ovbiagele B, Black HR, Bravata DM, Chimowitz MI, Ezekowitz MD, et al. Guidelines for the prevention of stroke in patients with stroke and transient ischemic attack: A guideline for healthcare professionals from the american heart association/american stroke Association. Stroke. 2014;45:2160–236.
29. Fujimoto K, Norikane T, Yamamoto Y, Takami Y, Mitamura K, Okada M, et al. Association between carotid 18F-NaF and 18F-FDG uptake on PET/CT with ischemic vascular brain disease on MRI in patients with carotid artery disease. Ann Nucl Med. 2019;33:907–15.
30. Norikane T, Yamamoto Y, Maeda Y, Okada M, Nishiyama Y. Correlation of noninvasive imaging of vulnerable carotid artery plaque using NaF and FDG PET/CT and black-blood MRI with cerebral ischemia on brain MRI. J Nucl Med. 2018;59:40–40.
31. Vengrenyuk Y, Carlier S, Xanthos S, Cardoso L, Ganatos P, Virmani R, et al. A hypothesis for vulnerable plaque rupture due to stress-induced debonding around cellular microcalcifications in thin fibrous caps. Proc Natl Acad Sci. 2006;103:14678–83.
32. Kelly-Arnold A, Maldonado N, Laudier D, Aikawa E, Cardoso L, Weinbaum S. Revised microcalcification hypothesis for fibrous cap rupture in human coronary arteries. Proc Natl Acad Sci. 2013;110:10741–6.
33. Roijers RB, Debernardi N, Cleutjens JPM, Schurgers LJ, Mutsaers PHA, van der Vusse GJ. Microcalcifications in early intimal lesions of atherosclerotic human coronary arteries. Am J Pathol. 2011;178:2879–87.
34. den Harder AM, Wolterink JM, Bartstra JW, Spiering W, Zwakenberg SR, Beulens JW, et al. Vascular uptake on 18F-sodium fluoride positron emission tomography: Precursor of vascular calcification? J Nucl Cardiol. 2020. https://doi.org/10.1007/s12350-020-02031-5.
35. Murshed M, Harmey D, Millán JL, McKee MD, Karsenty G. Unique coexpression in osteoblasts of broadly expressed genes accounts for the spatial restriction of ECM mineralization to bone. Genes Dev. 2005;19:1093–104.
36. Sheen CR, Kuss P, Narisawa S, Yadav MC, Nigro J, Wang W, et al. Pathophysiological role of vascular smooth muscle alkaline phosphatase in medial artery calcification: Role of TNAP in medial vascular calcification. J Bone Miner Res. 2015;30:824–36.
37. Libby P. Inflammation in atherosclerosis. Arterioscler Thromb Vasc Biol. 2012;32:2045–51.
38. Arbab-Zadeh A, Fuster V. The Myth of the ''Vulnerable Plaque''. J Am Coll Cardiol. 2015;65:846–55.
39. Chung AG, Frye JB, Zbesko JC, Constantopoulos E, Hayes M, Figueroa AG, et al. Liquefaction of the brain following stroke shares a similar molecular and morphological profile with atherosclerosis and mediates secondary neurodegeneration in an osteopontin-dependent mechanism. Eneuro. 2018;5:ENEURO.0076.

40. Lee YS, Kim JS, Kim KM, Kang JH, Lim SM, Kim H-J. Performance measurement of PSF modeling reconstruction (True X) on siemens biograph TruePoint TrueV PET/CT. Ann Nucl Med. 2014;28:340–8.
41. Schramm G, Maus J, Hofheinz F, Petr J, Lougovski A, Beuthien-Baumann B, et al. Correction of quantification errors in pelvic and spinal lesions caused by ignoring higher photon attenuation of bone in [18 F]NaF PET/MR. Med Phys. 2015;42:6468–76.
42. Kelly PJ, Camps-Renom P, Giannotti N, Martí-Fàbregas J, McNulty JP, Baron J-C, et al. A risk score including carotid plaque inflammation and stenosis severity improves identification of recurrent stroke. Stroke. 2020;51:838–45.
43. Debray J, Chang L, Marquès S, Pellet-Rostaing S, Le Duy D, Mebarek S, et al. Inhibitors of tissue-nonspecific alkaline phosphatase: Design, synthesis, kinetics, biomineralization and cellular tests. Bioorg Med Chem. 2013;21:7981–7.